Journal of Alloys and Compounds 509 (2011) 4470–4477

Contents lists available at ScienceDirect

Journal of Alloys and Compounds

journal homepage: www.elsevier.com/locate/jallcom

Experimental determination of the phase equilibria in the Co–Fe–Zr ternary system

C.P. Wang[a], Y. Yu[a], H.H. Zhang[a], H.F. Hu[b], X.J. Liu[a,*]

[a] Department of Materials Science and Engineering, College of Materials, and Research Center of Materials Design and Applications, Xiamen University, Xiamen 361005, PR China
[b] Baosteel Group Shanghai Meishan Co., Ltd., Nanjing 210039, PR China

ARTICLE INFO

Article history:
Received 18 October 2010
Received in revised form
30 December 2010
Accepted 4 January 2011
Available online 13 January 2011

Keywords:
Metal and alloys
Phase diagrams
X-ray diffraction

ABSTRACT

The phase equilibria in the Co–Fe–Zr ternary system were investigated by means of optical microscopy (OM), electron probe microanalysis (EPMA), X-ray diffraction (XRD), and differential scanning calorimetry (DSC) on equilibrated ternary alloys. Four isothermal sections of the Co–Fe–Zr ternary system at 1300 °C, 1200 °C, 1100 °C and 1000 °C were experimentally established. The experimental results indicate that (1) no ternary compound was found in this system; (2) the solubility of Fe in the liquid phase of the Co-rich corner at 1300 °C is extremely large; (3) the liquid phase in the Zr-rich corner and the $(Co,Fe)_2Zr$ phase form the continuous solid solutions from the Co–Zr side to the Fe–Zr side; (4) the solubility of Zr in the fcc (Co, Fe) phase is extremely small.

1. Introduction

The Co–Fe base alloys are important magnetic materials in applications of electronic industry, information technology and recording media [1,2]. The Co–Fe–Zr system is one of important subsystems for the typical magnetic metallic materials. In addition, the Co–Fe–Zr base alloys are also used as high temperature materials and amorphous materials [3–5]. For the advanced development of high-performance Co–Fe–Zr base alloys, accurate information on the phase equilibria in the Co–Fe–Zr system is especially required. Although the isothermal sections at 500 °C investigated by Mishenina et al. [6] and at 1000 °C determined by Raghavan [7] were available, however, there are still two main conflicts in the isothermal section at 1000 °C (shown in Fig. 1), which are summarized as follows: (1) the existence of the $FeZr_2$ phase at 1000 °C is obviously not in accordance with that in the Fe–Zr binary phase diagram (presented in Fig. 2) reviewed by Okamoto [8] and (2) the chemical compositions of the Fe_3Zr phase has a big difference from that in Ref. [8]. Therefore, it is important and necessary to comprehensively determine the phase equilibria in the Co–Fe–Zr ternary system.

In the Co–Fe–Zr ternary system, the Co–Fe [9], Co–Zr [10–12] and Fe–Zr [8] three sub-binary systems have been experimentally investigated. The Co–Fe phase diagram is characterized by an extremely narrow solidification range. The fcc continuous solid solution exists from the fcc (Fe) phase to the fcc (Co) phase over a wide range of temperature [9]. In the Co–Zr phase diagram, there are five intermediate phases: $Co_{11}Zr_2$, $Co_{23}Zr_6$, Co_2Zr, CoZr and $CoZr_2$ [10]. Later, Bataleva et al. [11] confirmed the existence of the $CoZr_3$ phase. Among these, Co_2Zr and $CoZr_3$ phases have a range of homogeneity. The main information of the Co–Zr phase diagram is obtained by Pechin et al. [10] and our work [12]. The Fe–Zr system reviewed by Okamoto [8] shows that the stable phases are the liquid phase, terminal solid solutions δFe, αFe, γFe, βZr, and αZr, and four intermetallic compounds, namely, $Fe_{23}Zr_6$, Fe_2Zr, $FeZr_2$, and $FeZr_3$ phases. Nine invariant reactions exist in the system involving all the phases mentioned above. The phase diagram in the Co–Fe [9], Co–Zr [10] and Fe–Zr [8] three sub-binary systems are shown in Fig. 2. The information of the stable solid phases in the three binary systems mentioned above is summarized in Table 1.

Recently, our group has been focused on developing a thermodynamic database of the phase diagrams in the Co-based alloys [13–21]. In order to obtain the detailed information of phase equilibria for the thermodynamic assessment, the objective of the present work is to experimentally determine the isothermal sections at 1300 °C, 1200 °C, 1100 °C and 1000 °C using the equilibrated ternary alloys, which will meet the need for the thermodynamic description of the Co–Fe–Zr ternary system and provide a better understanding of microstructures of promising alloys for practical applications.

2. Experimental procedure

Cobalt (99.8 wt.%), iron (99.9 wt.%) and zirconium (99.7 wt.%) were used as starting materials. Bulk buttons were prepared from pure elements by arc melting under

* Corresponding author. Tel.: +86 592 2187888; fax: +86 592 2187966.
E-mail address: lxj@xmu.edu.cn (X.J. Liu).

0925-8388/$ – see front matter © 2011 Elsevier B.V. All rights reserved.
doi:10.1016/j.jallcom.2011.01.030

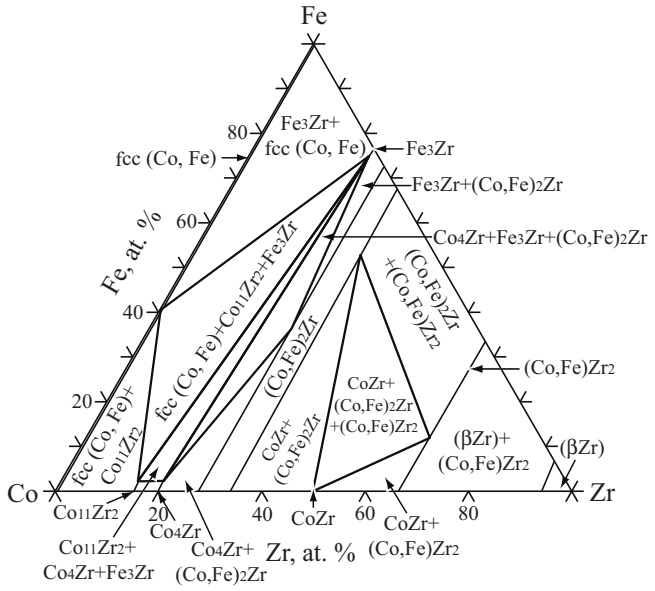

Fig. 1. The isothermal section of the Co–Fe–Zr system at 1000 °C reviewed by Raghavan [7].

high purity argon atmosphere using a non-consumable tungsten electrode. The ingots were melted at least five times in order to achieve their homogeneity. The sample weight is around 20 g and the weight loss during melting is generally less than 0.20% of the sample weight. Afterwards, the ingots were cut into small pieces for heat treatments and further observations.

The specimens were wrapped in Mo foil in order to prevent direct contact with the quartz ampoule, and put into quartz evacuated and backfilled with argon gas. The specimens were annealed in temperature range between 1000 °C and 1300 °C, respectively. The time of the heat treatment varied from several hours to 3 months depending on temperature and composition of the specimen. At the end of the heat treatment, the specimens were quenched into ice water.

After standard metallographic preparation, the microstructural observations were carried out by optical microscopy (OM) and scanning electron microscopy (SEM). The reliable equilibrium compositions of each phase were determined by electron probe microanalysis (EPMA) (JXA-8100R, JEOL, Japan) based on the wavelength dispersive spectroscopy (WDS) and pure elements cobalt, iron and zirconium were used as standard materials. The conditions of measurements were 20.0 kV for voltage and 10 nA for beam current, respectively. The equilibrium compositions were obtained by averaging the compositions determined by EPMA.

The X-ray diffraction (XRD) was used to identify the crystal structure of the constituent phases. The X-ray powder diffraction patterns of the experimental samples were carried out on a Phillips Panalytical X-pert diffractometer using Cu Kα radiation at 40 kV and 30 mA. The data were collected in the range of 2θ from 20° to 90° at a step width of 0.0167°. The differential scanning calorimetry (DSC) method was used to determine the temperature of phase transformation. Al_2O_3 power was used as reference substance. The heating and cooling rates were both set to 10 °C/min. All measurements were conducted under argon atmosphere.

3. Results and discussion

3.1. Microstructure

The BSE (back-scattered electron) images of the typical ternary alloys for the Co–Fe–Zr system are presented in Fig. 3(a)–(h). Phase identification was based on equilibrium composition measured by EPMA. The $Co_{80}Fe_{13}Zr_7$ (at.%) and $Co_{50}Fe_{10}Zr_{40}$ (at.%) alloys annealed at 1300 °C for 1 h and 6 days are respectively located in the two-phase regions (liquid + fcc (Co, Fe)) and (CoZr + $(Co,Fe)_2Zr$), as characterized in Fig. 3(a) and (b), respectively. The fcc (Co, Fe) phase and the $(Co,Fe)_2Zr$ phase distribute in the matrix of the liquid phase and CoZr phase, respectively. In the $Co_{87}Fe_6Zr_7$ (at.%) alloy quenched from 1200 °C, the two phases $Co_{11}Zr_2$ and fcc (Co, Fe) were identified, as shown in Fig. 3(c). The three-phase equilibrium of the liquid + $(Co,Fe)_2Zr$ + CoZr were identified in the $Co_{30}Fe_{20}Zr_{50}$ (at.%) alloys quenched from 1200 °C for 6 h, as indicated in Fig. 3(d). The $Co_{40}Fe_{45}Zr_{15}$ (at.%) and $Co_{35}Fe_3Zr_{62}$ (at.%) annealed at 1100 °C for 3 months are located in the three-phase region of the $Fe_{23}Zr_6$ + fcc (Co, Fe) + $(Co,Fe)_2Zr$ and two-phase region of the CoZr + $CoZr_2$, as shown in Fig. 3(e–f). In addition, the two-phase equilibrium of the $(Co,Fe)_2Zr$ + $CoZr_2$ and three-phase equilibrium of the $CoZr_2$ + $(Co,Fe)_2Zr$ + CoZr were identified

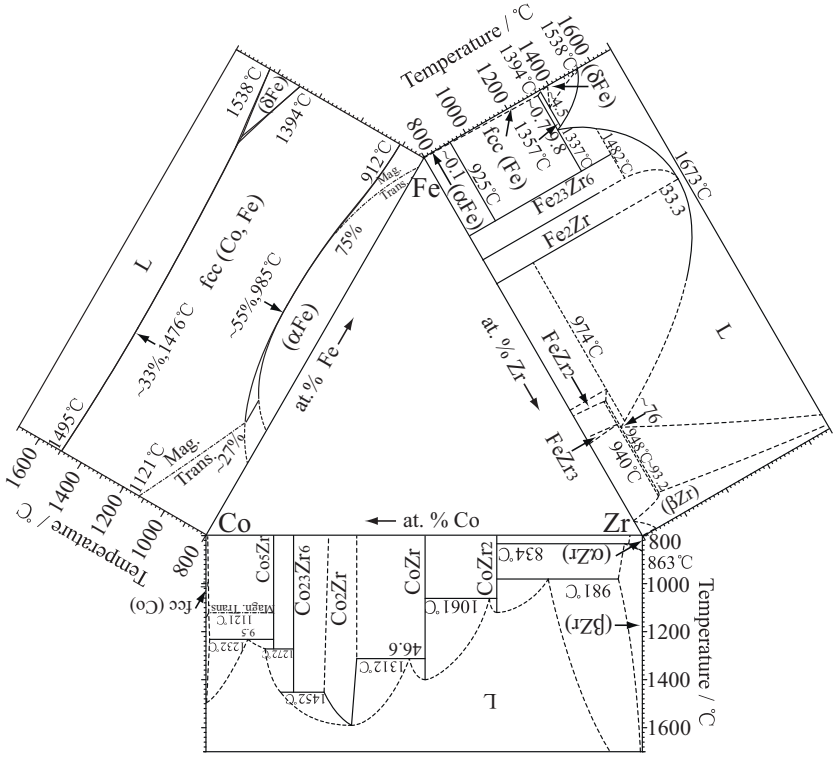

Fig. 2. Binary phase diagrams constituting the Co–Fe–Zr ternary system [8–10].

Table 1
The stable phases in the three binary systems.

System	Phase	Pearson's symbol	Prototype	Struktur-bericht	References
Co–Fe	fcc (Co, Fe)	cF4	Cu	A1	[8]
	(αFe)	c12	W	A2	[8]
	(δFe)	c12	W	A2	[8]
Co–Zr	fcc (Co)	cF4	Cu	A1	[9]
	(εCo)	hP2	Mg	A3	[9]
	$Co_{23}Zr_6$	cF116	$Mn_{23}Th_6$	$D8_2$	[9]
	Co_2Zr	cF24	Cu_2Mg	C15	[9]
	CoZr	cP2	CsCl	B2	[9]
	$CoZr_2$	Ti12	Al_2Cu	C16	[9]
	(βZr)	C12	W	A2	[9]
	(αZr)	hP2	Mg	A3	[9]
	$CoZr_3$	oC16	Re_3B	$E1_{12}$	[9]
Fe–Zr	(αZr)	hP2	Mg	A3	[12]
	(βZr)	C12	W	A2	[12]
	$FeZr_3$	oC16	Re_3B	$E1_{12}$	[12]
	$FeZr_2$	Ti12	Al_2Cu	C16	[12]
	Fe_2Zr	cF24	Cu_2Mg	C15	[12]
	$Fe_{23}Zr_6$	cF116	$Mn_{23}Th_6$	$D8_2$	[12]
	(αFe)	c12	W	A2	[12]
	fcc (Fe)	cF4	Cu	A1	[12]
	(δFe)	c12	W	A2	[12]

in the $Co_{12}Fe_{38}Zr_{50}$ (at.%) and $Co_{25}Fe_{30}Zr_{45}$ (at.%) alloys annealed at 1000 °C for 4 months, respectively, and indicated in Fig. 3(g) and (h), respectively.

3.2. Structure and melting points

The $Co_{50}Fe_{10}Zr_{40}$ (at.%) alloy annealed at 1300 °C for 6 days was substantiated by the XRD experiment, as shown in Fig. 4(a), where the characteristic peaks of the $(Co,Fe)_2Zr$ and CoZr phases are well distinguished by different symbols, which are consistent with the results determined by EPMA, as shown in Fig. 3(b). In addition, the XRD result of $Co_{25}Fe_{30}Zr_{45}$ (at.%) alloy quenched from 1000 °C is shown in Fig. 4(b), where the characteristic peaks of the CoZr, $CoZr_2$ and $(Co,Fe)_2Zr$ were marked by different symbols, which is observed in Fig. 3(h).

The DSC analysis was performed in order to determined the melting points of three different alloys $Co_6Fe_{19}Zr_{75}$ (at.%), $Co_{12}Fe_{13}Zr_{75}$ (at.%) and $Co_{19}Fe_6Zr_{75}$ (at.%). Their DSC curves on heating are presented in Fig. 5, respectively. It can be known that the appearance of the liquid phase in the Zr-rich corner is below 1000 °C, which indicates that there should be a liquid phase from Co–Zr side to Fe–Zr side at 1000 °C.

3.3. Isothermal section

The equilibrium compositions of the Co–Fe–Zr ternary system at 1300 °C, 1200 °C, 1100 °C and 1000 °C determined by EPMA are listed in Tables 2–5, respectively.

Based on these experimental data mentioned above, the isothermal sections at 1300 °C, 1200 °C, 1100 °C and 1000 °C were

Table 2
Equilibrium compositions of the Co–Fe–Zr system at 1300 °C.

Alloy (at.%)	Equilibria	Composition (at.%)					
	Phase 1/phase 2/phase 3	Phase 1		Phase 2		Phase 3	
		Fe	Zr	Fe	Zr	Fe	Zr
$Co_{40}Fe_{10}Zr_{50}$	$(Co,Fe)_2Zr$/CoZr/liquid	24.09	32.61	9.32	48.55		12.39
$Co_{40}Fe_{20}Zr_{40}$	$(Co,Fe)_2Zr$/CoZr	26.45	32.29	5.08	48.78		
$Co_{40}Fe_{35}Zr_{25}$	$Fe_{23}Zr_6$/$(Co,Fe)_2Zr$	40.83	20.19	33.60	25.49		
$Co_{40}Fe_{45}Zr_{15}$	Liquid/$Fe_{23}Zr_6$	51.98	8.54	38.82	20.33		
$Co_{60}Fe_{30}Zr_{10}$	fcc (Co, Fe)/liquid	40.35	2.17	27.58	10.19		
$Co_{60}Fe_{21}Zr_{19}$	Liquid/$Co_{23}Zr_6$	28.14	9.89	20.19	19.72		
$Co_{60}Fe_{15}Zr_{25}$	$Co_{23}Zr_6$/$(Co,Fe)_2Zr$	16.92	21.23	13.57	25.58		
$Co_{10}Fe_{80}Zr_{10}$	fcc (Co, Fe)/$Fe_{23}Zr_6$	89.50	0.14	66.78	19.81		
$Co_{50}Fe_{40}Zr_{10}$	fcc (Co, Fe)/liquid	50.19	0.35	36.97	10.33		
$Co_{65}Fe_{23}Zr_{12}$	Liquid/$Co_{23}Zr_6$	23.89	10.97	13.64	20.54		
$Co_{80}Fe_{13}Zr_7$	fcc (Co, Fe)/liquid	14.10	0.02	7.79	10.04		
$Co_{87}Fe_6Zr_7$	fcc (Co, Fe)/liquid	8.05	0.14	4.85	9.16		
$Co_7Fe_{43}Zr_{50}$	$(Co,Fe)_2Zr$/liquid	63.04	31.71	24.20	65.23		
$Co_{12}Fe_{38}Zr_{50}$	$(Co,Fe)_2Zr$/liquid	58.14	32.24	18.91	65.13		
$Co_{25}Fe_{30}Zr_{45}$	$(Co,Fe)_2Zr$/CoZr/liquid	42.77	33.57	10.46	49.95	12.45	64.58
$Co_{30}Fe_{20}Zr_{50}$	$(Co,Fe)_2Zr$/CoZr/liquid	40.39	32.46	9.69	48.96	13.09	63.20
$Co_{50}Fe_{10}Zr_{40}$	$(Co,Fe)_2Zr$/CoZr	12.45	32.26	2.38	49.18		
$Co_{55}Fe_5Zr_{40}$	$(Co,Fe)_2Zr$/CoZr	8.02	32.31	1.05	49.03		
$Co_{35}Fe_3Zr_{62}$	CoZr/liquid	2.89	48.61	3.92	65.43		
$Co_{70}Fe_5Zr_{25}$	$Co_{23}Zr_6$/$(Co,Fe)_2Zr$	6.59	20.24	3.78	25.49		
$Co_{35}Fe_{40}Zr_{25}$	$Fe_{23}Zr_6$/$(Co,Fe)_2Zr$	46.42	20.21	39.70	25.39		
$Co_7Fe_{68}Zr_{25}$	$Fe_{23}Zr_6$/$(Co,Fe)_2Zr$	73.14	20.23	67.88	25.45		
$Co_{6.7}Fe_{3.3}Zr_{90}$	Liquid/(βZr)	1.76	84.41	0.20	97.00		
$Co_{3.3}Fe_{6.7}Zr_{90}$	Liquid/(βZr)	9.67	83.76	2.63	96.76		

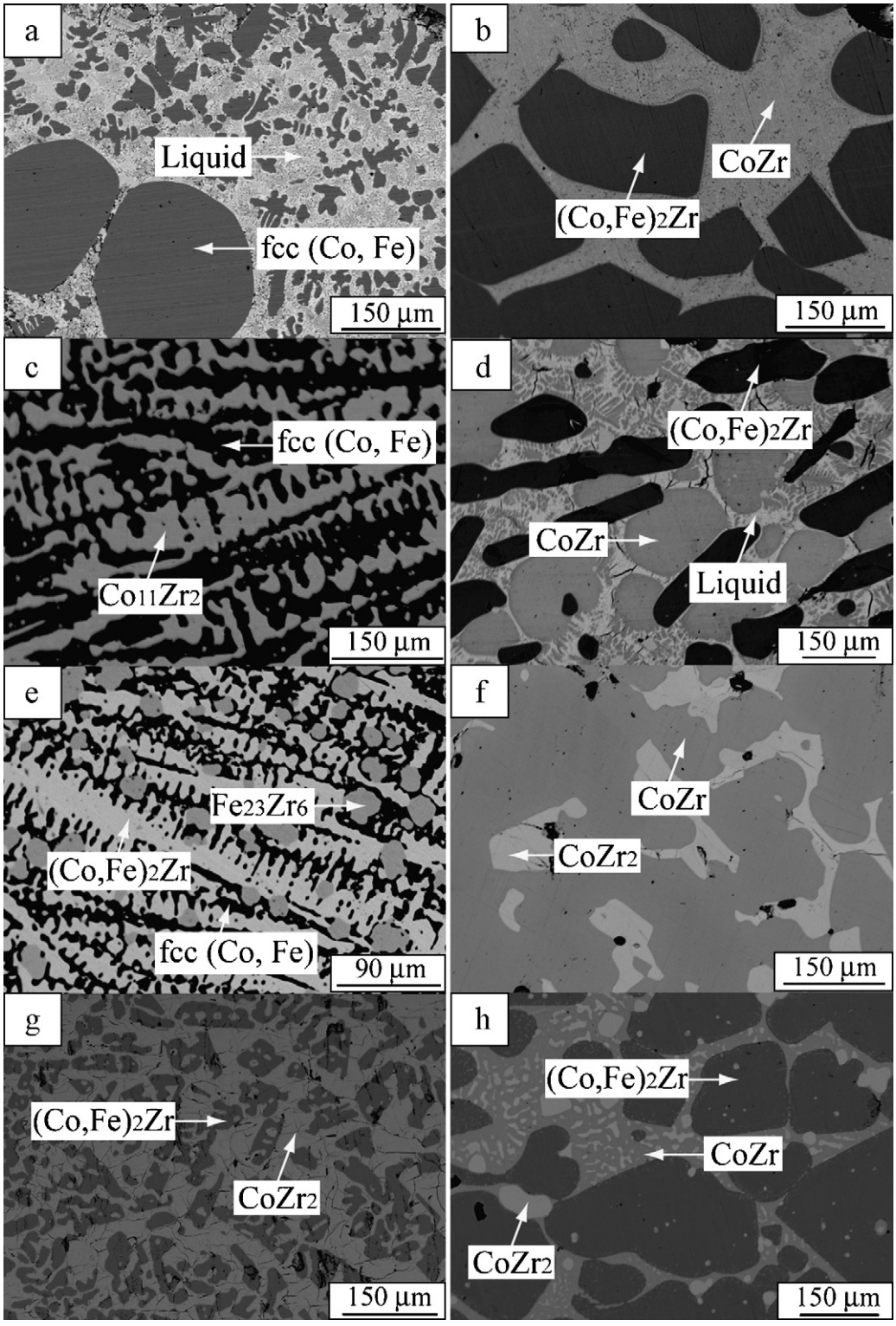

Fig. 3. BSE images of typical ternary alloys: (a) $Co_{80}Fe_{13}Zr_7$ (at.%) alloy annealed at 1300 °C for 1 h; (b) $Co_{50}Fe_{10}Zr_{40}$ (at.%) alloy annealed at 1300 °C for 6 days; (c) $Co_{87}Fe_6Zr_7$ (at.%) alloy annealed at 1200 °C for 1 month; (d) $Co_{30}Fe_{20}Zr_{50}$ (at.%) alloy annealed at 1200 °C for 6 h; (e) $Co_{40}Fe_{45}Zr_{15}$ (at.%) alloy annealed at 1100 °C for 3 months; (f) $Co_{35}Fe_3Zr_{62}$ (at.%) alloy annealed at 1100 °C for 3 months; (g) $Co_{12}Fe_{38}Zr_{50}$ (at.%) alloy annealed at 1000 °C for 4 months; (h) $Co_{25}Fe_{30}Zr_{45}$ (at.%) alloy annealed at 1000 °C for 4 months.

constructed in Fig. 6(a)–(d). Fig. 6(a) shows the isothermal section at 1300 °C, where the solubility of Zr in the fcc (Co, Fe) phase is extremely small and the solubility of Fe in liquid phase of the Co-rich corner is extremely large. In addition, the liquid phase in the Zr-rich corner and the $(Co,Fe)_2Zr$ phase form the continuous solid solutions from the Co–Zr side to the Fe–Zr side. The three-phase equilibrium ($CoZr + (Co,Fe)_2Zr$ + liquid), rather than ternary compound was identified. Three three-phase equilibria, fcc (Co, Fe) + liquid + $Fe_{23}Zr_6$, liquid + $(Co,Fe)_2Zr$ + $Fe_{23}Zr_6$ and liquid + $(Co,Fe)_2Zr$ + $Co_{23}Zr_6$, as shown in Fig. 5(a) in dashed lines, were

Table 3
Equilibrium compositions of the Co–Fe–Zr system at 1200 °C.

Alloy (at.%)	Equilibria	Composition (at.%)					
	Phase 1/phase 2/phase 3	Phase 1		Phase 2		Phase 3	
		Fe	Zr	Fe	Zr	Fe	Zr
$Co_{40}Fe_{10}Zr_{50}$	$(Co,Fe)_2Zr/CoZr$/Liquid	40.25	32.47	8.75	48.58	13.56	65.07
$Co_{40}Fe_{20}Zr_{40}$	$(Co,Fe)_2Zr/CoZr$	28.67	32.54	4.75	49.10		
$Co_{40}Fe_{35}Zr_{25}$	$Fe_{23}Zr_6/(Co,Fe)_2Zr$	40.55	19.92	33.83	25.37		
$Co_{40}Fe_{45}Zr_{15}$	fcc (Co, Fe)/$Fe_{23}Zr_6$/$(Co,Fe)_2Zr$	61.83	0.26	38.06	19.65	32.37	23.66
$Co_{60}Fe_{30}Zr_{10}$	fcc (Co, Fe)/$Co_{23}Zr_6$	37.20	0.07	19.23	20.24		
$Co_{60}Fe_{21}Zr_{19}$	fcc (Co, Fe)/$Co_{23}Zr_6$	35.49	0.39	18.20	20.61		
$Co_{60}Fe_{15}Zr_{25}$	$Co_{23}Zr_6/(Co,Fe)_2Zr$	19.10	20.19	14.61	25.82		
$Co_{10}Fe_{80}Zr_{10}$	fcc (Co, Fe)/$Fe_{23}Zr_6$	90.18	0.06	66.16	20.68		
$Co_{20}Fe_{70}Zr_{10}$	fcc (Co, Fe)/$Fe_{23}Zr_6$	80.23	0.03	47.85	20.03		
$Co_{30}Fe_{63}Zr_7$	fcc (Co, Fe)/$Fe_{23}Zr_6$	70.55	0.07	43.12	20.76		
$Co_{50}Fe_{40}Zr_{10}$	fcc (Co, Fe)/$(Co,Fe)_2Zr$	47.23	0.08	17.54	24.08		
$Co_{65}Fe_{23}Zr_{12}$	fcc (Co, Fe)/$Co_{23}Zr_6$	28.60	0.05	13.82	20.13		
$Co_{80}Fe_{13}Zr_7$	fcc (Co, Fe)/$Co_{11}Zr_2$	15.42	0.01	6.24	15.26		
$Co_{87}Fe_6Zr_7$	fcc (Co, Fe)/$Co_{11}Zr_2$	6.55	0.13	2.54	15.18		
$Co_7Fe_{43}Zr_{50}$	$(Co,Fe)_2Zr$/liquid	62.78	32.63	23.21	66.98		
$Co_{12}Fe_{38}Zr_{50}$	$(Co,Fe)_2Zr$/liquid	58.57	31.62	19.64	64.73		
$Co_{25}Fe_{30}Zr_{45}$	$(Co,Fe)_2Zr/CoZr$/liquid	41.69	31.60	9.09	49.75	13.87	65.93
$Co_{30}Fe_{20}Zr_{50}$	$(Co,Fe)_2Zr/CoZr$/liquid	40.72	31.83	8.56	48.15	13.99	64.35
$Co_{50}Fe_{10}Zr_{40}$	$(Co,Fe)_2Zr/CoZr$	15.13	31.45	1.77	48.60		
$Co_{55}Fe_5Zr_{40}$	$(Co,Fe)_2Zr/CoZr$	7.37	32.41	0.74	49.08		
$Co_{35}Fe_3Zr_{62}$	CoZr/liquid	2.91	48.87	3.87	63.82		
$Co_{70}Fe_5Zr_{25}$	$Co_{23}Zr_6/(Co,Fe)_2Zr$	5.43	20.75	4.11	24.24		
$Co_{35}Fe_{40}Zr_{25}$	$Fe_{23}Zr_6/(Co,Fe)_2Zr$	41.95	20.14	37.06	25.27		
$Co_7Fe_{68}Zr_{25}$	$Fe_{23}Zr_6/(Co,Fe)_2Zr$	73.05	20.24	66.63	25.50		
$Co_{70}Fe_{11}Zr_{19}$	$Co_{11}Zr_2/Co_{23}Zr_6$	10.71	15.38	9.95	20.00		
$Co_{6.7}Fe_{3.3}Zr_{90}$	Liquid/(βZr)	6.76	76.24	1.12	96.76		
$Co_{3.3}Fe_{6.7}Zr_{90}$	Liquid/(βZr)	15.30	78.16	2.35	96.09		

still not determined. In the isothermal section at 1200 °C (Fig. 6(b)), two three-phase equilibria, CoZr + $(Co,Fe)_2Zr$ + liquid and fcc (Co, Fe) + $(Co,Fe)_2Zr$ + $Fe_{23}Zr_6$ were determined. The solubility of Zr in the $Co_{23}Zr_6$ phase is larger than that in the $Co_{11}Zr_2$ phase. The liquid phase in the Co-rich corner disappears, but the liquid phase in the Zr-rich corner still form the continuous solid solutions from the Co–Zr side to the Fe–Zr side. As shown in Fig. 6(c), the solid $CoZr_2$ phase, existing only below 1200 °C in the Co–Zr binary system [10–12], appears in the isothermal section at 1100 °C. The solubility of Fe in the $CoZr_2$ phase was found to be extremely large. Three three-phase equilibria, CoZr + $(Co,Fe)_2Zr$ + $CoZr_2$, fcc (Co, Fe) + $(Co,Fe)_2Zr$ + $Fe_{23}Zr_6$ and fcc (Co, Fe) + $Co_{11}Zr_2$ + $Co_{23}Zr_6$

Table 4
Equilibrium compositions of the Co–Fe–Zr system at 1100 °C.

Alloy (at.%)	Equilibria	Composition (at.%)					
	Phase 1/phase 2/phase 3	Phase 1		Phase 2		Phase 3	
		Fe	Zr	Fe	Zr	Fe	Zr
$Co_{40}Fe_{10}Zr_{50}$	$(Co,Fe)_2Zr/CoZr$	32.17	34.32	5.66	50.54		
$Co_{40}Fe_{20}Zr_{40}$	$(Co,Fe)_2Zr/CoZr$	28.85	32.84	4.32	49.01		
$Co_{40}Fe_{35}Zr_{25}$	$Fe_{23}Zr_6/(Co,Fe)_2Zr$	38.42	19.16	31.95	25.22		
$Co_{40}Fe_{45}Zr_{15}$	fcc (Co, Fe)/$Fe_{23}Zr_6$/$(Co,Fe)_2Zr$	61.39	0.08	37.07	19.70	31.67	23.35
$Co_{60}Fe_{30}Zr_{10}$	fcc (Co, Fe)/$Co_{23}Zr_6$	40.45	0.48	18.73	20.32		
$Co_{60}Fe_{21}Zr_{19}$	fcc (Co, Fe)/$Co_{23}Zr_6$	38.11	0.30	16.49	20.25		
$Co_{60}Fe_{15}Zr_{25}$	$Co_{23}Zr_6/(Co,Fe)_2Zr$	20.45	20.04	14.91	25.35		
$Co_{10}Fe_{80}Zr_{10}$	fcc (Co, Fe)/$Fe_{23}Zr_6$	90.43	0.69	62.02	20.39		
$Co_{20}Fe_{70}Zr_{10}$	fcc (Co, Fe)/$Fe_{23}Zr_6$	81.97	0.41	50.17	20.65		
$Co_{30}Fe_{63}Zr_7$	fcc (Co, Fe)/$Fe_{23}Zr_6$	70.51	0.19	43.08	20.37		
$Co_{50}Fe_{40}Zr_{10}$	fcc (Co, Fe)/$(Co,Fe)_2Zr$	49.95	0.33	22.30	23.15		
$Co_{65}Fe_{23}Zr_{12}$	fcc (Co, Fe)/$Co_{23}Zr_6$	32.68	0.11	11.51	20.05		
$Co_{80}Fe_{13}Zr_7$	fcc (Co, Fe)/$Co_{11}Zr_2$	17.02	0.12	6.88	15.24		
$Co_{87}Fe_6Zr_7$	fcc (Co, Fe)/$Co_{11}Zr_2$	7.79	0.04	2.80	15.34		
$Co_7Fe_{43}Zr_{50}$	$(Co,Fe)_2Zr/CoZr_2$	62.75	31.52	22.67	6545		
$Co_{12}Fe_{38}Zr_{50}$	$(Co,Fe)_2Zr/CoZr_2$	58.59	32.14	20.02	63.75		
$Co_{25}Fe_{30}Zr_{45}$	$(Co,Fe)_2Zr/CoZr/CoZr_2$	50.41	30.72	12.54	48.18	15.15	62.14
$Co_{30}Fe_{20}Zr_{50}$	$(Co,Fe)_2Zr/CoZr/CoZr_2$	50.87	31.05	13.06	48.16	15.65	63.15
$Co_{50}Fe_{10}Zr_{40}$	$(Co,Fe)_2Zr/CoZr$	15.15	32.08	1.61	48.29		
$Co_{55}Fe_5Zr_{40}$	$(Co,Fe)_2Zr/CoZr$	7.75	31.48	0.82	48.41		
$Co_{35}Fe_3Zr_{62}$	$CoZr/CoZr_2$	2.91	48.25	3.20	68.51		
$Co_{72.5}Fe_{7.5}Zr_{20}$	$Co_{11}Zr_2/Co_{23}Zr_6$	7.79	15.34	4.62	21.05		
$Co_{35}Fe_{40}Zr_{25}$	fcc (Co, Fe)/$(Co,Fe)_2Zr$	45.58	19.51	38.63	25.39		
$Co_7Fe_{68}Zr_{25}$	$Fe_{23}Zr_6/(Co,Fe)_2Zr$	73.90	18.96	67.08	25.14		
$Co_{70}Fe_{11}Zr_{19}$	fcc (Co, Fe)/$Co_{11}Zr_2$/$Co_{23}Zr_6$	20.74	1.49	11.08	15.01	7.39	20.97
$Co_{6.7}Fe_{3.3}Zr_{90}$	Liquid/(βZr)	7.71	75.58	13.37	96.75		
$Co_{3.3}Fe_{6.7}Zr_{90}$	Liquid/(βZr)	19.10	75.24	0.13	97.82		

Table 5
Equilibrium compositions of the Co–Fe–Zr system at 1000 °C.

Alloy (at.%)	Equilibria	Composition (at.%)					
	Phase 1/phase 2/phase 3	Phase 1		Phase 2		Phase 3	
		Fe	Zr	Fe	Zr	Fe	Zr
$Co_{40}Fe_{10}Zr_{50}$	$CoZr/CoZr_2$	9.29	48.72	12.44	64.02		
$Co_{40}Fe_{20}Zr_{40}$	$(Co,Fe)_2Zr/CoZr$	28.73	32.67	4.01	49.52		
$Co_{40}Fe_{35}Zr_{25}$	$Fe_{23}Zr_6/(Co,Fe)_2Zr$	41.49	20.83	33.36	26.17		
$Co_{40}Fe_{45}Zr_{15}$	fcc (Co, Fe)/$Fe_{23}Zr_6$/$(Co,Fe)_2Zr$	63.45	0.26	38.33	20.40	30.97	23.94
$Co_{60}Fe_{30}Zr_{10}$	fcc (Co, Fe)/$Co_{23}Zr_6$	40.34	0.38	18.57	20.34		
$Co_{60}Fe_{15}Zr_{25}$	$Co_{23}Zr_6/(Co,Fe)_2Zr$	20.35	19.94	14.76	24.06		
$Co_{10}Fe_{80}Zr_{10}$	fcc (Co, Fe)/$Fe_{23}Zr_6$	90.91	0.11	66.39	20.81		
$Co_{20}Fe_{70}Zr_{10}$	fcc (Co, Fe)/$Fe_{23}Zr_6$	80.85	0.22	53.07	20.99		
$Co_{30}Fe_{63}Zr_7$	fcc (Co, Fe)/$Fe_{23}Zr_6$	70.02	0.24	42.77	20.24		
$Co_{50}Fe_{40}Zr_{10}$	fcc (Co, Fe)/$(Co,Fe)_2Zr$	48.86	0.17	20.45	24.28		
$Co_{65}Fe_{23}Zr_{12}$	fcc (Co, Fe)/$Co_{23}Zr_6$	32.77	0.89	11.11	21.25		
$Co_{80}Fe_{13}Zr_7$	fcc (Co, Fe)/$Co_{23}Zr_6$	15.81	0.08	4.83	19.19		
$Co_{87}Fe_6Zr_7$	fcc (Co, Fe)/$Co_{11}Zr_2$	7.17	0.04	2.65	15.52		
$Co_7Fe_{43}Zr_{50}$	$(Co,Fe)_2Zr/CoZr_2$	66.25	29.91	27.71	63.37		
$Co_{12}Fe_{38}Zr_{50}$	$(Co,Fe)_2Zr/CoZr_2$	62.26	30.35	18.97	64.58		
$Co_{25}Fe_{30}Zr_{45}$	$(Co,Fe)_2Zr/CoZr/CoZr_2$	43.35	31.85	13.89	49.24	12.98	65.73
$Co_{30}Fe_{20}Zr_{50}$	$(Co,Fe)_2Zr/CoZr/CoZr_2$	45.18	32.00	14.13	49.33	10.84	65.18
$Co_{50}Fe_{10}Zr_{40}$	$(Co,Fe)_2Zr/CoZr$	16.29	32.64	1.50	49.34		
$Co_{55}Fe_5Zr_{40}$	$(Co,Fe)_2Zr/CoZr$	8.82	31.80	7.42	48.69		
$Co_{35}Fe_3Zr_{62}$	$CoZr/CoZr_2$	3.65	49.68	2.89	65.79		
$Co_{70}Fe_5Zr_{25}$	$Co_{23}Zr_6/(Co,Fe)_2Zr$	7.53	21.09	4.77	25.47		
$Co_{35}Fe_{40}Zr_{25}$	$Fe_{23}Zr_6/(Co,Fe)_2Zr$	46.22	19.61	38.60	23.06		
$Co_7Fe_{68}Zr_{25}$	$Fe_{23}Zr_6/(Co,Fe)_2Zr$	73.67	20.12	66.85	25.29		
$Co_{70}Fe_{11}Zr_{19}$	fcc (Co, Fe)/$Co_{23}Zr_6$	21.42	0.56	6.73	20.94		
$Co_{6.7}Fe_{3.3}Zr_{90}$	Liquid/(βZr)	8.16	75.05	1.75	96.23		
$Co_{3.3}Fe_{6.7}Zr_{90}$	Liquid/(βZr)	16.25	75.17	3.27	95.89		

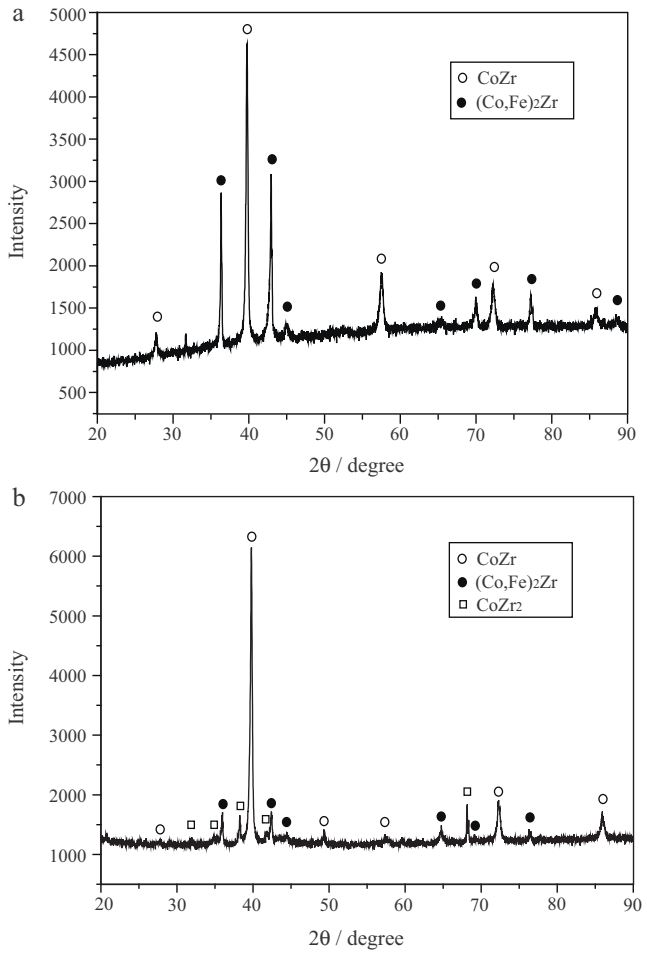

Fig. 4. X-ray diffraction patterns obtained from (a) $Co_{50}Fe_{10}Zr_{40}$ (at.%) alloy annealed at 1300 °C for 6 days and (b) $Co_{25}Fe_{30}Zr_{45}$ (at.%) alloy annealed at 1000 °C for 4 months.

were determined and three three-phase equilibria shown in dashed line were still not determined. In the isothermal section at 1000 °C (Fig. 6(d)), the liquid phase was found to still exist in the Zr-rich corner and formed the continuous solutions from the Co–Zr side to Fe–Zr side, which also corresponds to the results of DSC analysis mentioned above, showing that the temperature of liquid phase of the Zr-rich corner appears at about 985 °C. The isothermal section at 1000 °C determined in present work is different from 1000 °C investigated by Raghavan [7] (Fig. 1). In the present work, the melting point of the $FeZr_2$ phase was determined to be about 955.6 °C, which indicated that the $FeZr_2$ phase does not exist at 1000 °C. Thus, the continuous solid solution of $(Co,Fe)Zr_2$ phase does not exist at 1000 °C.

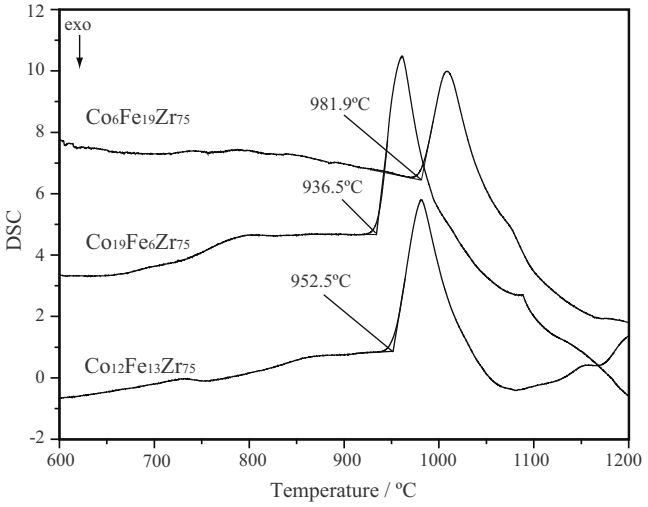

Fig. 5. DSC heating curves of the $Co_6Fe_{19}Zr_{75}$ (at.%), $Co_{19}Fe_6Zr_{75}$ (at.%) and $Co_{12}Fe_{13}Zr_{75}$ (at.%) alloys.

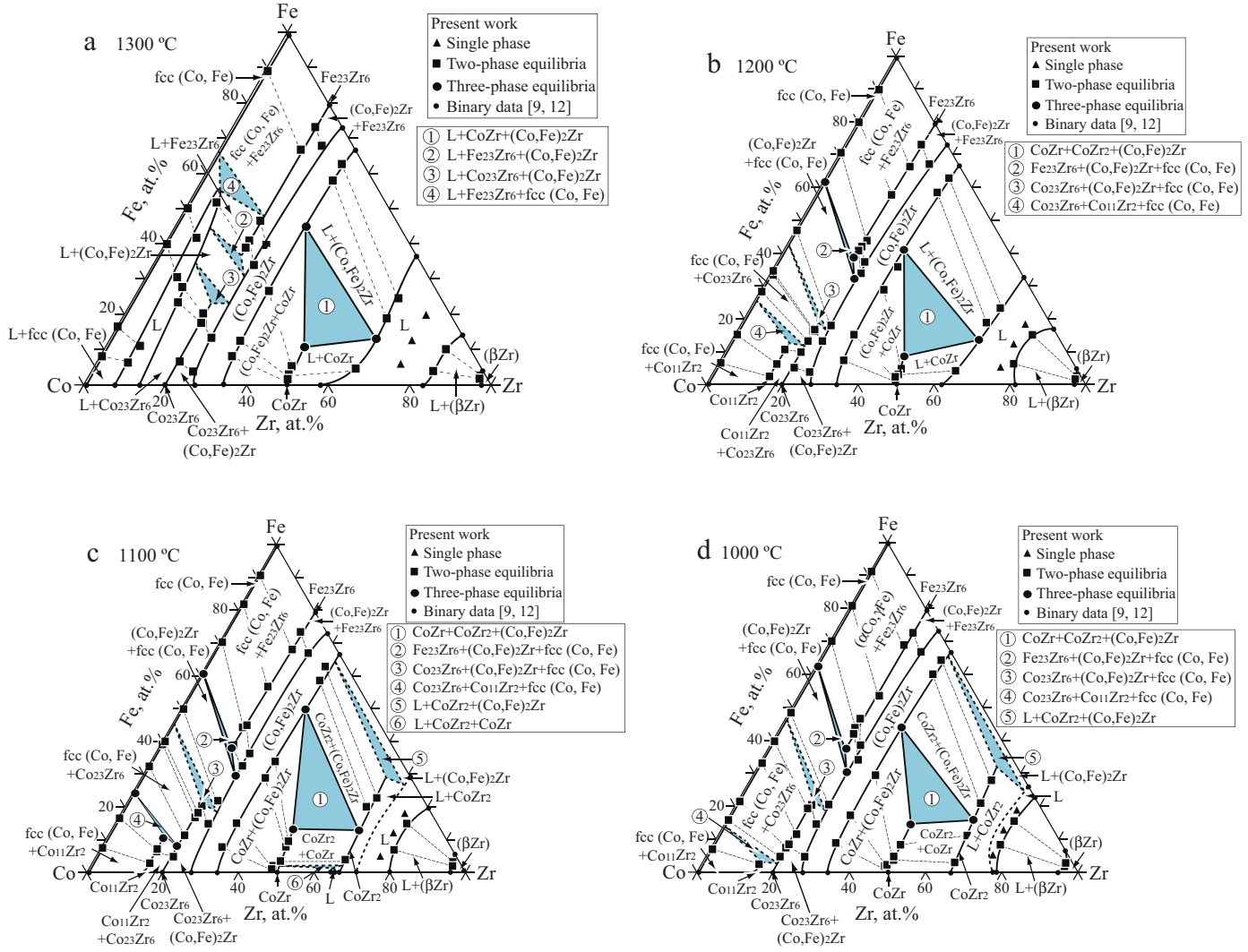

Fig. 6. Experimentally determined isothermal sections of the Co–Fe–Zr system: (a) 1300 °C; (b) 1200 °C; (c) 1100 °C; (d) 1000 °C.

4. Conclusions

Four isothermal sections of the Co–Fe–Zr ternary system at 1300 °C, 1200 °C, 1100 °C and 1000 °C were experimentally determined using equilibrated ternary alloys. The obtained experimental results show that: (1) the solubility of Fe in liquid phase of Co-rich corner at 1300 °C is extremely large; (2) the liquid phase of Zr-rich corner and the $(Co,Fe)_2Zr$ phase form the continuous solid solutions from the Co–Zr side to the Fe–Zr side; (3) the solubility of Zr in fcc (Co, Fe) phase is extremely small; (4) no ternary compound was found in this system.

The newly determined phase equilibria of the Co–Fe–Zr ternary system will provide additional support for the thermodynamic assessment of this system in the underway work and practical application for the amorphous alloys.

Acknowledgements

This work was supported by the National Natural Science Foundation of China (Grant Nos. 51031003, 50771088, 50971109), the Ministry of Science and Technology of China (Grant Nos. 2009DFA52170 and 2009AA03Z101). The Support from Fujian Provincial Department of Science & Technology (Grant No. 2009I0024), Xiamen City Department of Science & Technology (Grant No. 3502Z20093001), and Aviation Science Fund (Grant No. 2009ZF68010) are acknowledged.

References

[1] V.K. Dugaev, Y. Vygranenko, M.M. Vieira, Physica E 16 (2003) 558–562.
[2] R.C. Sousa, I.L. Prejbeanu, C. R. Phys. 6 (2005) 1013–1021.
[3] M. Zatroch, P. Petrovič, I. Brovko, T. Švec, M. Konč, J. Magn. Magn. Mater. 112 (1992) 334–336.
[4] L. Peng, Q.H. Yang, H.W. Zhang, G.L. Xu, M. Zhang, J.D. Wang, J. Rare Earths 26 (2008) 378–382.
[5] R.Z. Gong, X. Wang, W.M. Cheng, X. Shen, Mater. Lett. 62 (2008) 266–268.
[6] I.V. Mishenina, E.F. Kazakova, E.M. Sokolovskaya, N.Y. Tolmacheva, Moscow Univ. Chem. Bull. 51 (1996) 52–54.
[7] V. Raghavan, Ind. Inst. Met. 6 (1992) 681–686.
[8] H. Okamoto, J. Phase Equilib. 14 (1993) 652–653.
[9] I. Ohnuma, H. Enoki, O. Ikeda, R. Kainuma, H. Ohtani, B. Sundman, K. Ishida, Acta Mater. 50 (2002) 379.
[10] W.H. Pechin, D.E. Williams, W.L. Larsen, Trans. ASM 57 (1964) 464–473.
[11] S.K. Bataleva, V.V. Kuprina, V.V. Burnasheva, V.Y. Markiv, G.N. Ronami, S.M. Kurnetsova, Moscow Univ. Chem. Bull. 25 (1970) 33–36.
[12] X.J. Liu, H.H. Zhang, C.P. Wang, K. Ishida, J. Alloys Compd. 482 (2009) 99–105.
[13] C.P. Wang, X.J. Liu, I. Ohnuma, R. Kainuma, K. Ishida, J. Alloys Compd. 438 (2007) 129–141.
[14] C.P. Wang, J. Wang, X.J. Liu, I. Ohnuma, R. Kainuma, K. Ishida, J. Alloys Compd. 453 (2008) 174–179.
[15] C.P. Wang, P. Yu, X.J. Liu, I. Ohnuma, R. Kainuma, K. Ishida, J. Alloys Compd. 457 (2008) 150–156.

[16] X.J. Liu, P. Yu, C.P. Wang, K. Ishida, J. Alloys Compd. 466 (2008) 169–175.
[17] Y. Yu, C.P. Wang, X.J. Liu, I. Ohnuma, R. Kainuma, K. Ishida, Intermetallics 16 (2008) 1199–1205.
[18] J. Wang, X.J. Liu, C.P. Wang, J. Nucl. Mater. 374 (2008) 76–89.
[19] C.P. Wang, J. Wang, S.H. Guo, X.J. Liu, I. Ohnuma, R. Kainuma, K. Ishida, Intermetallics 17 (2009) 642–650.
[20] C.P. Wang, A.Q. Zheng, X.J. Liu, K. Ishida, J. Alloys Compd. 478 (2009) 197–201.
[21] X.J. Liu, Z.P. Jiang, C.P. Wang, K. Ishida, J. Alloys Compd. 478 (2009) 287–296.